ORIGINAL ARTICLE

WILEY bioTROPICA · ASSOCIATION FOR TROPICAL BIOLOGY AND CONSERVATION

Patterns and controls on island-wide aboveground biomass accumulation in second-growth forests of Puerto Rico

Sebastián Martinuzzi[1,2] | Bruce D. Cook[2] | Eileen H. Helmer[3] | Michael Keller[3,4] | Dexter H. Locke[5] | Humfredo Marcano-Vega[6] | María Uriarte[7] | Douglas C. Morton[2]

[1]SILVIS Lab, Department of Forest and Wildlife Ecology, University of Wisconsin-Madison, Madison, Wisconsin, USA

[2]Biospheric Sciences Laboratory, NASA Goddard Space Flight Center, Greenbelt, Maryland, USA

[3]USDA Forest Service International Institute of Tropical Forestry, San Juan, Puerto Rico, USA

[4]Jet Propulsion Laboratory, California Institute of Technology, Pasadena, California, USA

[5]USDA Forest Service Northern Research Station, Baltimore Field Station, Baltimore, Maryland, USA

[6]USDA Forest Service Southern Research Station, Knoxville, Tennessee, USA

[7]Department of Ecology, Evolution & Environmental Biology, Columbia University, New York, New York, USA

Correspondence
Sebastián Martinuzzi, SILVIS Lab, Department of Forest and Wildlife Ecology, University of Wisconsin-Madison, 1630 Linden Drive, Madison, WI 53706, USA.
Email: martinuzzi@wisc.edu

Associate Editor: Ferry Slik

Handling Editor: Laura Schneider

Abstract

Understanding the heterogeneity of biomass accumulation in second-growth tropical forests following land use abandonment is important for informing ecosystem carbon models and forest restoration efforts. There is an urgent need for a broad sample of second-growth forests to enhance our knowledge of carbon accumulation in human-dominated landscapes, especially for older forests. Puerto Rico has predominantly second-growth forests, ranging in age from approximately 25 to more than 80 years. We used an island-wide sample of airborne lidar from the NASA Goddard Lidar, Hyperspectral, and Thermal (G-LiHT) Airborne Imager collected on March 2017, forest inventory data, and data on forest age, precipitation, soils, and land use to estimate aboveground biomass stocks in moist and wet, second-growth tropical forests. Biomass accumulation rates in Puerto Rico were lower, on average, than in other Neotropical forests. Median biomass across >16,700 ha of older second-growth forests was 105 Mg ha^{-1}, and sampled biomass rarely surpassed 250 Mg ha^{-1}. Differences in biomass by age were large and persistent across different substrates and land uses, with a plateau in the pattern of island-wide biomass accumulation after about 33 years. A spatial regression model showed that multiple factors were related to biomass accumulation, including time since abandonment, geologic substrate, past land use as coffee or pasture, precipitation, topographic wetness index, and slope. Our findings have important consequences for the total carbon storage and expected climate mitigation benefits of large-scale reforestation efforts, and highlight the value of airborne lidar for quantifying biomass variability in complex tropical landscapes.

Abstract in Spanish is available with online material.

KEYWORDS
carbon, forest succession, lidar, restoration, tropical forests

1 | INTRODUCTION

Tropical second-growth forests, or tropical forests that regenerate naturally after the cessation of human land uses such as pasture or agriculture, contribute to the global forest carbon sink (Pan et al., 2011) and provide key habitat for tropical species (Rozendaal et al., 2019). Whether net carbon and biodiversity benefits of second-growth tropical forests are large (e.g., Griscom et al., 2017) or small (e.g., Nunes,

Oliveira, Siqueira, Morton, & Souza, 2020) rests on three underlying assumptions. The first assumption is that the extent of second-growth forests is large and growing. It has been hypothesized that 70% of the world's tropical forests, including 28% of the Neotropical forests, are second-growth, and that their extent will expand as more land is abandoned (Chazdon et al., 2016; FAO, 2010). Second, long-term climate mitigation from reforestation assumes permanence (Griscom et al., 2017), a substantial departure from rotational land management common across the tropics (Hansen et al., 2020; Nunes et al., 2020). Third, these studies assume that biomass in second-growth tropical forests recover quickly, taking an average of 66 years to reach 90% of old-growth values (Poorter et al., 2016). However, forest regeneration rates are extremely variable, and the drivers of this variation across landscapes are poorly understood (Chazdon, 2014; Norden et al., 2015). Studies to characterize the patterns and controls of biomass recovery across heterogeneous landscapes are critical to test these underlying assumptions regarding second-growth forests in order to improve carbon modeling studies and tropical forest restoration efforts worldwide.

Knowledge of forest regeneration rates and controls comes almost entirely from studies using a limited number of field plots. For example, Letcher and Chazdon (2009) used a chronosequence of 23 forest plots regrowing from pasture. A recent synthesis across 45 sites and ~1500 forest plots in Neotropical forests found more than a 10-fold difference in biomass accumulation in the first 20 years of forest succession (from 20 to 225 Mg ha^{-1}, average 122 Mg ha^{-1}, or a net carbon uptake of 3.05 Mg C ha^{-1} yr^{-1}) (Poorter et al., 2016). The broad range of biomass accumulation rates corresponds to 25–85% of aboveground biomass in old-growth conditions in the first 20 years (Poorter et al., 2016). Previous studies show that forest regeneration rates can be affected by a variety of abiotic and biotic factors besides stand age, such as climate (Poorter et al., 2016), soils (Orihuela-Belmonte et al., 2013; Zarin et al., 2005), land use history and surrounding land cover (Aide, Zimmerman, Pascarella, Rivera, & Marcano-Vega, 2000; Aide, Zimmerman, Rosario, & Marcano, 1996; Arroyo-Rodríguez et al., 2017; Bonner, Schmidt, & Shoo, 2013; Crk, Uriarte, Corsi, & Flynn, 2009; Helmer et al., 2010; Zarin et al., 2005), topography (Crk et al., 2009; Orihuela-Belmonte et al., 2013), species composition (Lasky et al., 2014; Poorter et al., 2016), geological substrate (Helmer, Brandeis, Lugo, & Kennaway, 2008), and disturbance (Becknell et al., 2018; Flynn et al., 2010). Analysis of small (<1 ha) forest inventory plots demonstrated that site-specific factors complicate the interpretation of biomass recovery in second-growth forests (Norden et al., 2015). Because forest inventory plot data are costly and time-consuming to collect, it is difficult to capture landscape-scale variability, limiting our understanding of patterns and controls of biomass recovery. Consequently, large-scale studies of biomass accumulation are needed to capture gradients in environmental conditions and a diversity of forest ages, including older second-growth forests.

Lidar remote sensing captures three-dimensional forest structure and provides a unique opportunity to evaluate fine-scale variability in biomass recovery across large landscapes (Becknell et al., 2018; Mascaro, Asner, Dent, DeWalt, & Denslow, 2012). First, the combination of lidar and forest inventory data can be used to estimate aboveground forest biomass across the entire domain of airborne lidar coverage, including remote and fragmented landscapes rarely sampled with other techniques (Gobakken et al., 2012; Huang et al., 2019; Hudak et al., 2012). Second, combining predicted aboveground biomass with estimates of forest age derived from past land use data and satellite imagery increases the sample size for subsequent analyses of biomass accumulation by several orders of magnitude compared to data available from ground inventories (Becknell et al., 2018; Helmer, Lefsky, & Roberts, 2009). However, previous lidar-based studies of second-growth forests have primarily focused on protected areas, rather than more extensive human-dominated landscapes. For example, Becknell et al. (2018) quantified biomass recovery in Serra do Conduru State Park (Atlantic Forest, Brazil) and found rapid initial biomass regeneration (6 Mg ha^{-1} yr^{-1}) for forests between 10 and 32 years old, although biomass varied substantially within forests of similar age. A regression model that accounted for spatial autocorrelation and included forest age, slope, and distance to roads or open areas explained 62% of that variation (Becknell et al., 2018). In contrast to studies that used airborne lidar, Helmer et al. (2009) used satellite lidar data from the Geoscience Laser Altimeter System (GLAS) over Rondônia, Brazil, and found an average biomass accumulation rate of 8.4 Mg ha^{-1} yr^{-1} for forests of 3–16 years.

Puerto Rico is an ideal place to assess the patterns and controls of biomass accumulation in second-growth tropical forest landscapes following land use abandonment. First, the island has abundant second-growth forests of ~25 to 80+ yr, and therefore includes many examples of relatively mature forests that are less common in other Neotropical regions. Second, forests have recovered over different geologic substrates (e.g., volcanic and limestone), past land uses (e.g., coffee and pasture), and climates (e.g., moist and wet), which provides a unique opportunity to evaluate the role of multiple controls on biomass accumulation. Third, the island has a long history of forest research and monitoring through forest inventory plots, which are key inputs for remote sensing applications like biomass mapping.

Our goal was to understand the patterns and abiotic controls of aboveground biomass accumulation in second-growth tropical forest landscapes following land use abandonment on the main island of Puerto Rico. Specifically, our objectives were to: (i) quantify biomass and infer the rates of biomass accumulation based on time since abandonment in second-growth forest of Puerto Rico, and (ii) understand the main abiotic controls on rates of biomass accumulation. Using airborne lidar data, our study captured gradients in environmental conditions across the island, providing the fine-scale detail over large areas needed to characterize the variability of forest carbon stocks.

2 | METHODS

2.1 | Study area

The island of Puerto Rico is approximately 9000 km^2, of which 55% is forested, and most of the forests are the result of land abandonment (Franco, Weaver, & Eggen-McIntosh, 1997). The shift in the

island's economy from agricultural to manufacturing and services triggered widespread land abandonment in the 1940s. Forest cover increased rapidly in the 1950s and stabilized by 2000, after which time the rates of deforestation and regeneration of new second-growth forests were approximately equal (Helmer et al., 2008). As a result, there is a wide range of forest ages (5 to ~80 years), with most being older than 20 years (Figure 1a). The most common past land uses were coffee plantations and pastures, and to a lesser degree sugar cane plantations and other agriculture (Figure 1e) (Kennaway & Helmer, 2007).

At the same time, the island includes a variety of geologic substrates including volcaniclastic, limestone, intrusive, and others (Figure 1c). Elevation ranges from 0 to 1330 m, and annual precipitation varies from 701 mm to 4598 mm (Figure 1d). Most forests are subtropical moist or subtropical wet according to the Holdridge

Life Zone System (Figure 1b). We focused on the moist and wet forests from Holdridge (excluding the dry forests from our analysis), referred to here as humid forests, because these ecosystems have the highest carbon sequestration potential (Poorter et al., 2016) and account for the majority of forest cover on the island.

2.2 | Data

We developed two models to assess aboveground biomass in second-growth forests of Puerto Rico. First, we used co-located forest inventory and high-density airborne lidar data to calibrate a statistical model of aboveground forest biomass using metrics derived from airborne lidar data, which allowed us to map biomass within transects of lidar coverage across the island. Then, to understand
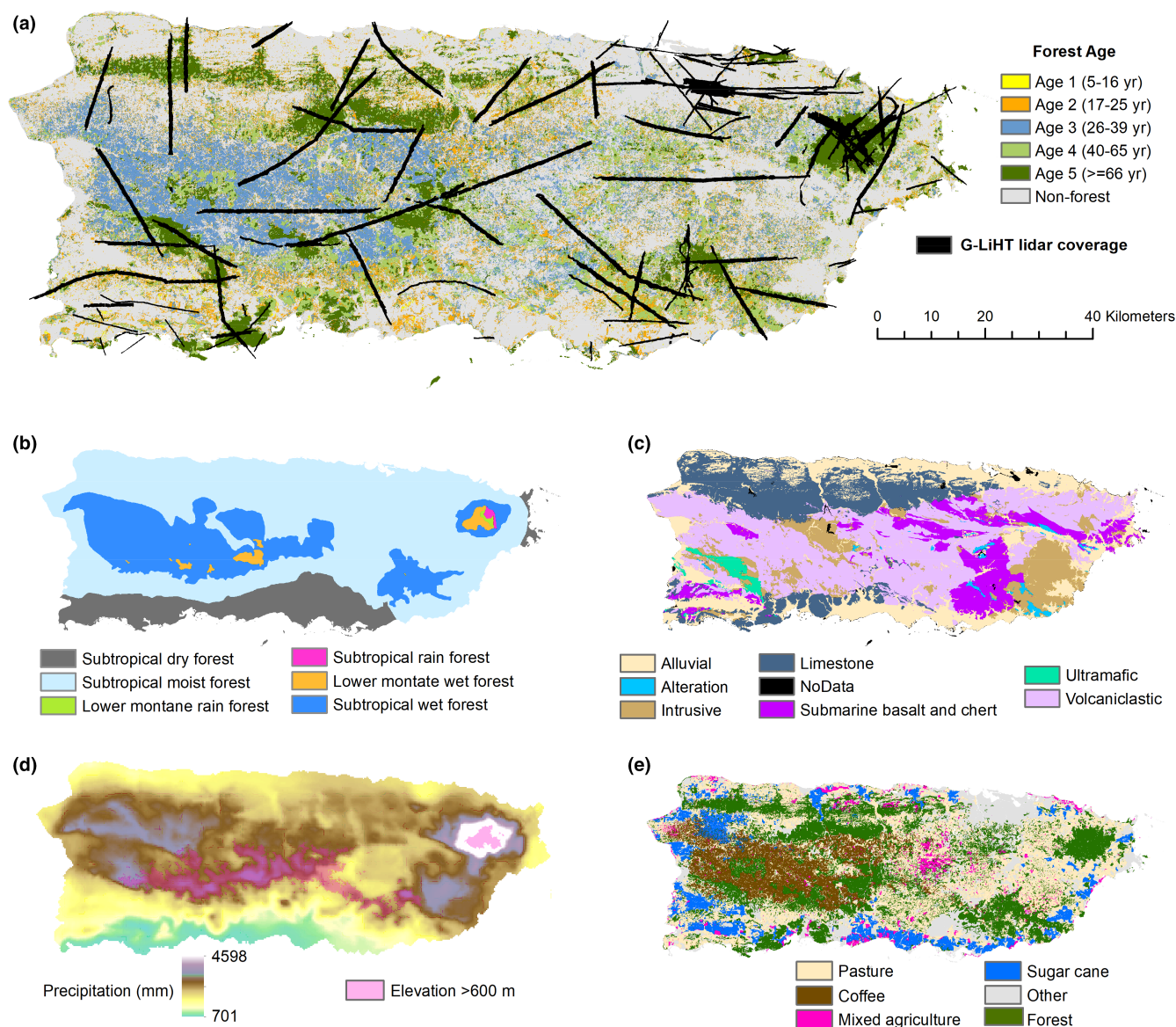

FIGURE 1 Study area and lidar acquisition areas. (a) Estimated forest age for the island of Puerto Rico, with G-LiHT lidar acquisitions shown in black; (b) Holdridge's life zones; (c) geologic substrate; (d) precipitation; (e) example of historic land use map (1977)

the rates and abiotic controls on biomass distributions, we evaluated the patterns of lidar-derived aboveground forest biomass across forest age classes and built a multivariate model of biomass accumulation with several environmental covariates. These two models are thus fundamentally different; while the goal of the first model is to predict (i.e., map) aboveground forest biomass, the goal of the second model is to understand the relationship between aboveground biomass and underlying environmental variables.

2.2.1 | Forest inventory data

We used data from permanent forest inventory plots from the U.S. Forest Inventory and Analysis (FIA) Program (hereafter "FIA plots"), which is a governmental program designed to monitor the forests of the United States, including Puerto Rico (Bechtold & Patterson, 2005; Woodall, Heath, Domke, & Nichols, 2011). The combination of FIA plots and airborne lidar data has proved useful for quantifying and mapping forest biomass in the conterminous United States (Ene et al., 2018; Nelson et al., 2017; Sheridan, Popescu, Gatziolis, Morgan, & Ku, 2015). FIA plots are systematically placed across the island, and each FIA plot consists of four circular subplots—a central subplot and three peripheral subplots—of 7.32-m radius each, sampling a total of 0.067 ha. All trees with a diameter at breast height (dbh) ≥ 12.7 cm are surveyed in each subplot. Each subplot includes a micro-plot of 2.1-m radius where all trees with a dbh of 2.54–12.7 cm are surveyed.

For calculating aboveground biomass (Mg ha^{-1}), the FIA Program uses two approaches. One approach uses regional allometric equations, and a second approach—called the component ratio method or CRM (Heath, Hansen, Smith, & Miles, 2009)—estimates aboveground biomass using separate allometric relationships and wood specific gravities for the tree bole, bark, stump, and crown. The CRM approach was designed to improve the consistency of biomass estimates across the nation. Although both estimates were highly correlated (Pearson correlation = 0.96), we used aboveground biomass (AGB) estimates calculated using the CRM approach because the overall model coefficient of determination was higher for the CRM approach.

We used FIA plots surveyed between 2016 and 2017, contemporary with the lidar acquisition (March 2017), and restricted our analysis to FIA plots in moist and wet forests for which all four subplots were covered by forest. Forest land according to the FIA Program is land that is at least 10% stocked by forest trees of any size and has a minimum area of 0.4 ha (Bechtold & Patterson, 2005). In addition, we excluded plots in mangroves and plots that were surveyed after the passage of Hurricane María in September 2017 to avoid confounding effects of hurricane damages. The final 56 plots used for calibration are located along the transects of lidar data shown in Figure 1a, and captured different forest ages, precipitation, geological substrate, and past land use (Figure 1). The location of FIA plots cannot be disclosed due to USFS policy. Aboveground biomass in the 56 FIA plots ranged from 4 to 243 Mg ha^{-1} with an average of 97 Mg ha^{-1}.

2.2.2 | Remote sensing data

We collected lidar data during March 2017 using NASA Goddard's LiDAR, Hyperspectral and Thermal (G-LiHT) Airborne Imager (Cook et al., 2013). G-LiHT data were acquired at a nominal altitude of 335 m using two synchronized Riegl VQ 480i scanning lidars at 300 kHz, providing a density of ≥12 pulses m^2, with up to eight returns per pulse. Lidar data were restricted to the central 30° field of view with a resulting swath width of 180 m. We collected lidar data along transects designed to capture the FIA plots used for calibration and sample the island's environmental heterogeneity (Figure 1a). Each transect consisted of three parallel transect lines with partial overlap. Coverage in some regions like El Yunque National Forest was more extensive to capture the network of existing research inventory plots. The G-LiHT data collection covered a total area of 51,611 ha of forest and non-forest, equivalent to 6% of the island area.

We calculated lidar metrics at 26-m pixel resolution (0.067 ha) to match the size of the FIA plots (i.e., the area sampled by the four subplots in each FIA plot). We calculated 54 lidar metrics of forest height (mean, standard deviation, skewness, and kurtosis), height percentiles, height densities, and lidar apparent reflectance, including different versions derived from all return heights, tree returns (returns above 1.37 m), shrub returns (returns below 1.37 m), ground returns, or the canopy height model (see Table S1 for a complete list, Cook et al., 2013). Identical lidar metrics were calculated for each FIA plot (n = 56) by clipping the lidar point cloud by the four subplot limits.

2.2.3 | Environmental data

We focused on six environmental variables known to influence forest regrowth in tropical landscapes and for which spatially explicit data exist for Puerto Rico: forest age, precipitation, geological substrate, past land use, topographic wetness, and slope (Pascarella, Aide, Serrano, & Zimmerman, 2000, Marcano-Vega, Aide, & Báez, 2002). The forest age map was developed by Helmer et al. (2008) by integrating historical land use maps from 1951 and 1977 derived from aerial photos with forest maps for the years 1991 and 2001 derived from Landsat satellite data. We extended these data with forest cover data from 2012 derived from Landsat data (Hansen et al., 2013), and used 2017 (i.e., the year of the lidar and FIA surveys) as the baseline year for calculating the forest age classes. This resulted in five forest age classes: 5–16, 17–25, 26–39, 40–65, and ≥66 years, Figure 1a), where the age classes are determined by the date of the historic forest maps. For example, the 5–16 years age class corresponds to 2017 forest pixels that appeared as forest in the 2012 map but appeared as non-forest in the 2001 map (i.e., min age is 2017–2012 = 5; max age is 2017–2001 = 16). The age intervals for each class are also different because they reflect the dates of the historic maps. Information on the most recent type of land use other than forest (i.e., coffee,

pasture, and sugar cane) was derived from the historic land use maps (Helmer et al., 2008), and assumed that coffee plantations in our period of study were shade coffee. Data on mean annual precipitation (averaged over 1963–1995) and geologic substrates came from Daly, Helmer, and Quiñones (2003) and Bawiec (1999), respectively. Topographic position influences forest structure and dynamics by affecting abiotic conditions like soil moisture and mechanical stability (Arriaga, 2000; Schwartz, Budsock, & Uriarte, 2019). We calculated the topographic wetness index (TWI) and slope from the lidar-derived digital terrain model at 26-m resolution using the package *dynatopmodel* in R (Metcalfe, Beven, & Freer, 2015). High TWI values indicate grid cells with topographical characteristics favorable for moisture accumulation, and slope affects both runoff and the type and location of human activities on the landscape. For example, flat, well-drained areas and more fertile soil types are typically cleared first for agriculture, whereas steep slopes and nutrient-poor soils are often the last sites to be cleared and the first to be abandoned. In our model, mean annual precipitation, geologic substrate, topographic wetness, and slope do not change through time.

2.3 | Analysis

2.3.1 | Lidar–biomass estimates

We estimated AGB using ordinary least-squares regression (OLS), a common approach in lidar–biomass applications (Andersen, Reutebuch, McGaughey, d'Oliveira, & Keller, 2014; Drake et al., 2002; Ene et al., 2018). We built a lidar–biomass OLS model based on the 56 FIA plots, with AGB as the dependent variable and the lidar metrics as predictor variables. We first used Pearson's correlations to eliminate highly correlated ($r > 0.9$) predictor variables, reducing the number of lidar predictor variables from 54 to 15 (see Table S1). Following Longo et al. (2016), we used the subset selection of regression method (Miller, 1984) to identify the best lidar metrics among the 15 variables. The subset selection of regression method identifies the most parsimonious model from a large number of predictor candidates. We applied the subset selection method using the function *regsubsets* (package *leaps* in R software) in the full model with exhaustive search and retained only the best subset of predictor variables among the previously chosen 15 variables. We used the Bayesian Information Criterion (BIC; Schwarz, 1978) to select the final model, that is, the model with the lowest BIC statistic.

To assess the accuracy of the model we used a 5-fold cross-validation repeated 100 times (package *caret*). Residuals from the final model were tested for linearity, homoscedasticity, correlation, and normality using the function *gvlma* in R. The results from these model tests were not statistically significant (*p*-value >0.05), indicating that linear model assumptions were acceptable. All statistical analyses were done with R version 3.5.1. As a last step, we mapped biomass on all lidar transects by applying the regression function to the 26-meter resolution gridded lidar data.

2.3.2 | Rates and controls of aboveground biomass accumulation

To evaluate the rates and controls of biomass accumulation, we used six spatially explicit environmental variables (forest age, precipitation, geological substrate, past land use, topographic wetness, and slope). These environmental layers were not used in the creation of the biomass map. For age, we used the mid-point year of each age class (i.e., 11, 21, 33, and 53 years) and assumed an average of 83 years for the oldest age class (i.e., mid-point between 66 and 100 years). For geological substrate and past land use, we grouped the classes with low spatial coverage (<5% of the study area) into a single class, "Other" and focused on five major geological substrates (intrusive, limestone, submarine basalt and chert, ultramafic, and volcaniclastic), and two past land uses (coffee vs. pasture). We also assigned a past land use = "forest" to our oldest class (83) since we did not have past land use information prior to 1951. Furthermore, we restricted our analyses of rates and controls of biomass accumulation to elevations below 600 m (see Figure 1d), corresponding to the height of the cloud level, because historic land use activities were concentrated at low elevations. Finally, because we were interested in forested areas, and the resolution of the biomass map was 26 m, we restricted our analysis to 26-m pixels with ≥80 forest cover, based on a 2-m resolution land cover map (NOAA, 2017). The final number of 26-m pixels used in these analyses was 248,343 (or 16,788 ha).

To quantify the rate of biomass accumulation based on time since abandonment we used the median biomass values across the different forest ages and summarized biomass accumulation as a function of age for the different geologic substrates and for the two predominant past land uses (i.e., pasture and coffee). Finally, for comparison with other neotropical studies, we compared our results of biomass accumulation with age against results from field plots in Poorter et al. (2016) using the Mann–Whitney *U* test. Specifically, we used 639 plots of moist and wet forests from Poorter et al. (2016) ranging in age from 5 to 100 years (i.e., consistent with our study), which we grouped following our age classes (11, 21, 33, 53, and 83 years).

To evaluate the controls of forest regrowth, we fit an OLS model with the biomass map as the dependent variable and the six environmental variables (forest age, precipitation, geological substrate, past land use, topographic wetness, and slope) as explanatory variables. The multivariate model allowed us to evaluate the combined effect of all variables. However, because the model's input data were spatial and continuous, we expected the OLS models' residuals would not be independent. The global Moran's I test using a Euclidean distance of 50 m to define neighboring pixels revealed significant spatial autocorrelation (Moran's I 0.51, $p < .00001$), so the Lagrange Multiplier test and the decision tree by Anselin (2005: pp 198–200) was applied to select an appropriate spatial model specification: spatial lag, spatial error, or a portmanteau test (SARMA; i.e., a combination of spatial lag and spatial error). The suggested form SARMA was selected. When testing for spatial autocorrelation, we evaluated the results using different distances to define neighboring pixels, including 50,

100, 200, and 300 m, and chose 50 m because it resulted in the spatial regression model with the highest pseudo-R-squared.

Because of the spatially lagged y term in the SARMA specification in the final model, the dependent variable is on both the left- and right-hand side of the equation (Eq. S1). This specification assumes that biomass in a pixel is related not only by the value of covariates in the unit, but also by covariate values in neighboring units. This arises if soil water from adjacent cells influences growth in the focal cell, or if tall species disperse from adjacent cells, influencing canopy height. A feedback is present, and the coefficients therefore cannot be interpreted in the typical manner (Bivand & Piras, 2015). The emanating or spillover effects, known as impacts, require a Markov chain Monte Carlo simulation to generate a distribution of estimates for direct, indirect, and total impacts. Total impacts are the sum of direct and indirect impacts, and we report on the direct and total impacts. Analyses were done with packages *spdep* and *spatialreg* in R.

3 | RESULTS

3.1 | Lidar–biomass estimates

The lidar–biomass model obtained through the subset selection method explained 70% of the variation in AGB in the FIA data (Adjusted R^2 = 0.70; n = 56) and had a cross-validated RMSE of 34.2 Mg ha^{-1}. The model included five lidar predictor variables: mean height, standard deviation, skewness, kurtosis, and canopy rugosity (Figure 2; Table S2). The first four variables were derived from all return heights, while canopy rugosity was calculated from the 1-m resolution canopy height model (see Table S1). The model somewhat underestimated values for plots with highest biomass (Figure 2), a typical feature in lidar–biomass relationships, given that stem diameter growth continues after height growth ceases. In addition, using small calibration plots (0.067 ha) in this study may also contribute to underestimation of higher AGB because a single large tree can lead to a high plot biomass. Finally, although there is evidence of multicollinearity (see Appendix S1), this should not be a problem here because the goal of this model is used to predict biomass from lidar data, and not to understand the role of the independent variables (Kutner, Nachtsheim, Neter, & Li, 2005).

Across more than 16,700 ha of forest at low elevation (<600 m asl) in Puerto Rico, the aboveground biomass averaged 109 ± 54 Mg ha^{-1}, with a median of 105 Mg ha^{-1} and 99th percentile of 251 Mg ha^{-1} (Figure 3). Across the extent of the lidar coverage, the full resolution (26 m) captures important spatial structure in AGB from topography in the karst region of northwest Puerto Rico (subset 1), patchy variability due to forest fragmentation and topography around El Yunque National Forest (subset 2), and fine-scale variability in estimated AGB from edge effects in the island interior near major population centers (subset 3). The data also exhibit a southwest–northeast gradient in AGB, consistent with the distribution of mean annual precipitation (Figure 1d), with larger patches of higher-biomass forest
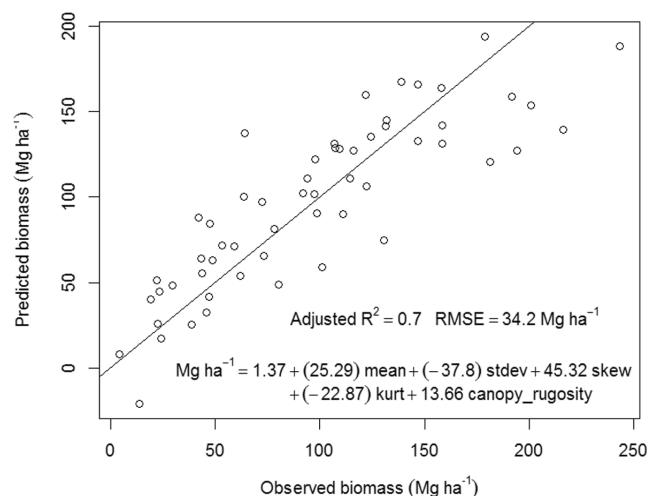

FIGURE 2 Predicted versus obserbed aboveground biomass, derived from lidar and forest inventory plots. See Table S1 for definitions of lidar metrics

in the island's interior, consistent with greater fragmentation and human impacts along the coastal margins (Figure 1a).

3.2 | Rates of and controls of biomass accumulation

Biomass increased rapidly during the first 33 years up to 109 Mg ha^{-1}, equivalent to an average rate of 3.3 Mg ha^{-1} yr^{-1}. Median AGB at 83 years was only 10% higher than at 33 years (120 vs. 109 Mg ha^{-1}, p < .0001; Figure 4a). This plateau in biomass accumulation in second-growth forests of Puerto Rico contrasts strongly with evidence for rapid biomass accumulation for at least 50 years in other Neotropical forests (Figure 4a). Biomass accumulation in Puerto Rico was 34% lower, on average, than the biomass accumulation by age estimated based on the data from Poorter et al. (2016), ranging between 11% lower in the youngest age class and 55% lower in the 53 years age class (Figure 4a).

Summarizing biomass across environmental layers revealed several important patterns in the relationship between biomass and age across geologic substrates. Biomass accumulation rates by age were lower on ultramafic than on intrusive, volcaniclastic, submarine basalt, and limestone substrates (Figure 4c). Median biomass by age did not show consistent increases on three substrates. On submarine basalt and volcaniclastic substrates, 53 years forests had lower median biomass than 33 years forests. Second-growth forests on ultramafic substrate had the slowest biomass accumulation, and intermediate-aged forests (33, 53 years) had higher biomass than the oldest forests (Figure 4c). Whereas average biomass reached 140 Mg ha^{-1} in intrusive and volcaniclastic substrates at age 83, biomass in ultramafic substrate peaked at age 33 with 78 Mg ha^{-1} (Figure 4d). These patterns for lower biomass at 53 years (submarine basalt and volcaniclastic) and 83 years (ultramafic) partially explain the apparent plateau in
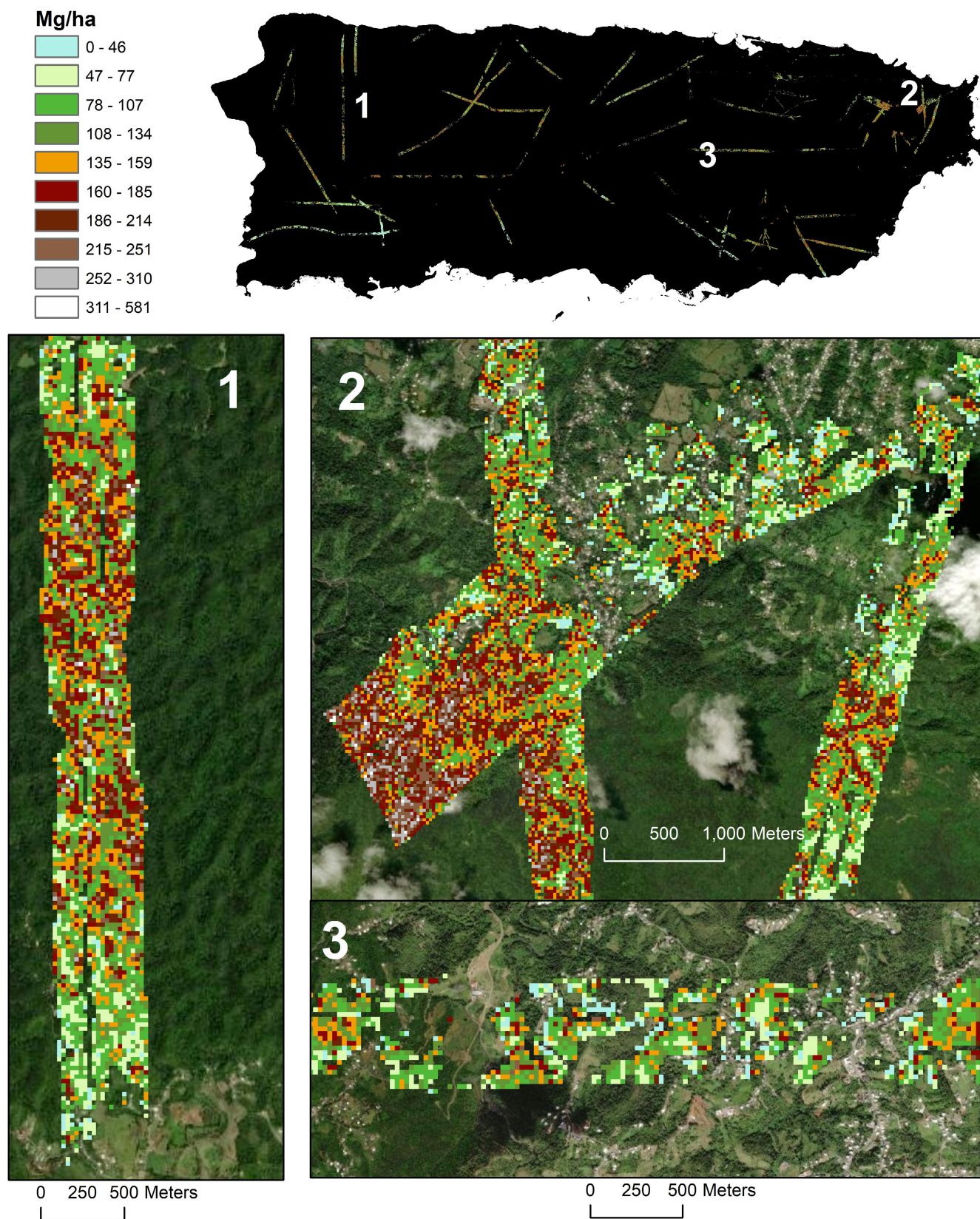
Mg/ha

- 0 - 46
- 47 - 77
- 78 - 107
- 108 - 134
- 135 - 159
- 160 - 185
- 186 - 214
- 215 - 251
- 252 - 310
- 311 - 581

FIGURE 3 Lidar-derived estimates of aboveground biomass at 26-m pixel resolution. Snapshots include (1) limestone; (2) El Yunque National Forest; (3) highly fragmented forest in the central part of the island

biomass accumulation after 33 years in the entire dataset, a pattern that is less apparent when looking at each substrate individually (Figure 4d).

Prior land use also influenced biomass accumulation in second-growth forests. Forests that recovered after coffee had 13–45% more biomass than those that recovered after pasture ($p < .0001$; Figure 4b).
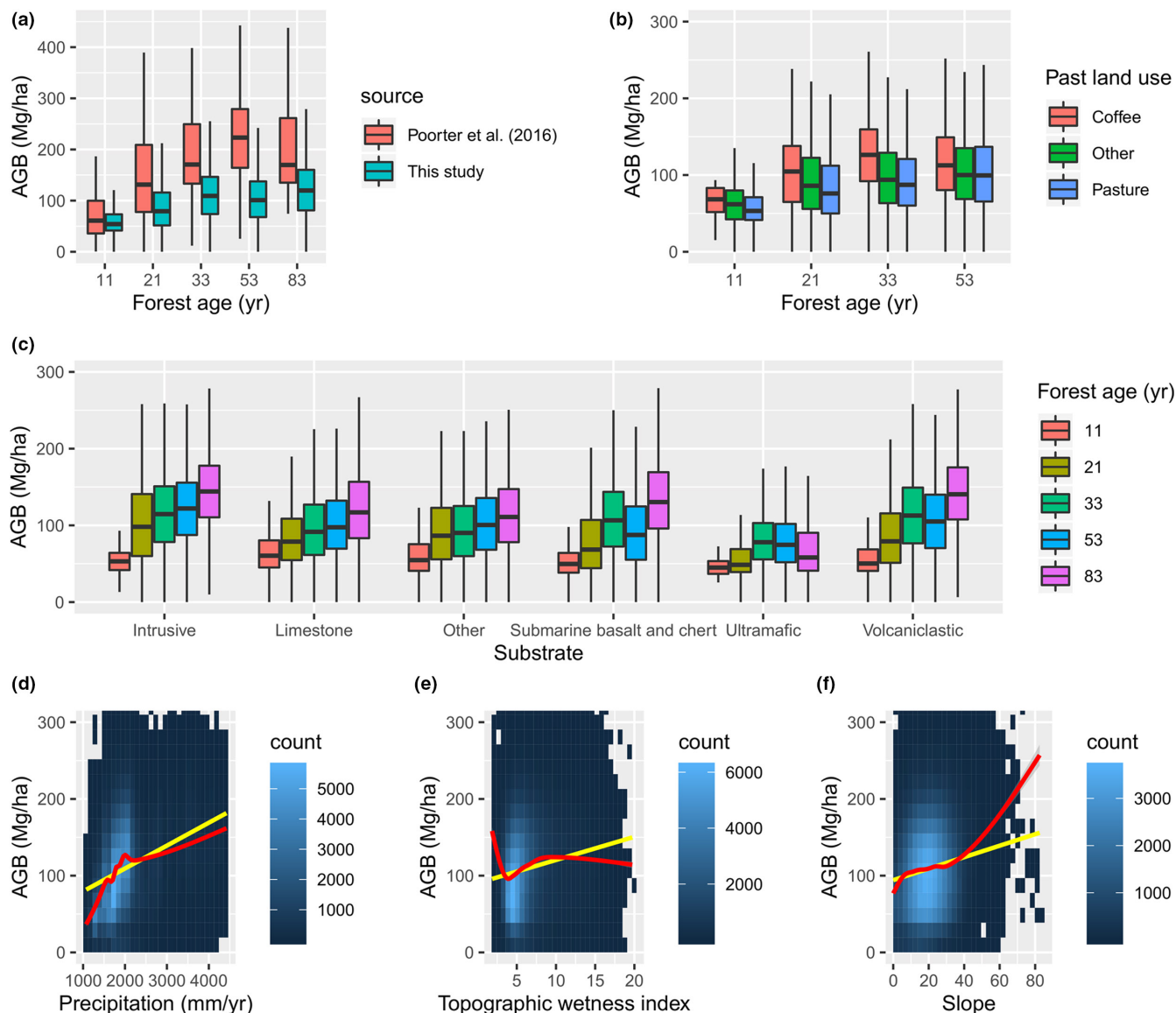
FIGURE 4 Distribution of biomass with age and across different environmental variables. (a) Biomass accumulation with age including the comparison with previous studies in the neotropics; (b) biomass accumulation based on past land use and (c) geologic substrate. (d-f) Relationship between biomass and precipitation, topographic wetness index, and slope. Yellow lines in panels d-f are the linear relationships; non-linear relationships (in red) are displayed for visualization purposes. The blue color in the background of figures d-f corresponds to the number of pixels (i.e., observations)

The only exception to this pattern was for the youngest age class (11 years, p-value = .263), but the sample size of younger forests following coffee was very low (n = 10 pixels) compared to other age/past land use combinations (n = 704 to 46,442 pixels). Biomass accumulation following other land uses (class "Other," including mixed agriculture, sugar cane, hay, and others) was intermediate between coffee and pasture (Figure 4b).

Finally, biomass in second-growth forests of Puerto Rico was linearly and positively associated (p < .0001) with mean annual precipitation (Figure 4d), topographic wetness (Figure 4e), and slope (Figure 4f), although the positive association between precipitation and biomass saturated above approximately 1800 mm yr^{-1}.

To evaluate the controls of forest regrowth we built a multivariate model using the environmental spatial layers. The AIC of the

spatial regression model was lower than the AIC for the linear model (2,486,700 vs 2,613,900), corroborating the use of a spatial regression model (Table 1). Further, both the spatial regression coefficient (ρ) and the simultaneous autoregressive error coefficient (λ) were highly significant (p < .00001), again confirming the appropriateness of model with both spatial lag and spatial error parameters.

Forest age, precipitation, topographic wetness, and slope all had positive direct impacts on biomass, while geological substrate and past land use had both positive and negative impacts (Table 1). Among geologic substrates, ultramafic had by far the most negative direct impact (−10.22 Mg ha^{-1}), while impacts varied slightly among the other substrates, from −1.89 Mg ha^{-1} in submarine basalt and chert to 2.15 Mg ha^{-1} in intrusive (Table 1). Among past land uses, coffee had a positive direct impact (5.19 Mg ha^{-1}), while pasture had

TABLE 1 OLS and spatial regression statistics

	OLS	Spatial regression			
	Estimate	Estimate	Direct Impact	Indirect Impact	Total Impact
(Intercept)	−16.81	−17.21			
Age	0.32	0.05	0.07	0.22	0.28
Precipitation	0.02	0.00	0.01	0.02	0.02
Substrate.Intrusive	8.11	1.70	2.15	6.91	9.05
Substrate.Limestone	1.12	0.07	0.08	0.27	0.35
Substrate.Submarine basalt and chert	−7.08	−1.49	−1.89	−6.07	−7.96
Substrate.Ultramafic	−40.88	−8.08	−10.22	−32.87	−43.09
Substrate.Volcaniclastic	−1.91	−0.04	−0.05	−0.17	−0.22
PastLandUse.Coffee	22.93	4.11	5.19	16.71	21.90
PatLandUse.Forest	2.35	0.63	0.79	2.55	3.35
PastLandUse.Pasture	−3.06	−0.65	−0.82	−2.63	−3.45
Topographic Wetness Index	5.30	2.51	3.17	10.21	13.38
Slope	1.38	0.51	0.64	2.07	2.72
Additional model statistics	RSE: 46.7	Rho: 0.81282, Lambda: −0.31833			
	Adj. *R*-squared: 0.2461	Nagelkerke pseudo-*R*-squared: 0.54841			
	AIC: 2613900	AIC: 2486700			

a negative impact ($-0.82 \, \mathrm{Mg\,ha^{-1}}$). The indirect impacts followed a similar pattern as the direct impacts, and these patterns were similar to those from the OLS model without a spatial component. Overall, the analysis of controls of biomass accumulation from the multivariate spatial model, multivariate OLS model, and visualizations of the individual factors provided consistent results showing contributions from age, substrate, past land use, and topographic wetness on biomass accumulation in second-growth forests of Puerto Rico.

4 | DISCUSSION

The integration of airborne lidar data, forest inventory plots, and spatial data on environmental and land use factors captured variability in biomass accumulation across more than 16,700 ha of second-growth forests in Puerto Rico. The large sample in this study, made possible based on high-density airborne lidar data, revealed complex spatial patterns of aboveground biomass, especially in older forests (≥53 years). Variability in aboveground biomass by forest age, geologic substrate, past land use, and topography underscores the complexity of natural and anthropogenic influences on forest recovery following land abandonment. Human-dominated landscapes are messy. Yet, landscape-scale studies of second-growth forests also capture important complexity in the rates of biomass accumulation needed to inform ecosystem models, forest restoration, and climate mitigation efforts.

Forest age is a strong predictor of AGB in second-growth forests, and yet forest age is a difficult parameter to quantify, based on

inherent challenges for estimating the timing of land abandonment, differences in initial conditions, and cumulative impacts of disturbance. Overall, the trajectory of biomass accumulation with forest age in this study followed the general patterns seen in previous work, especially for the period of rapid carbon accumulation in the first 20–30 years of regrowth. However, the influence of age uncertainty may be more pronounced in older second-growth forests. The airborne and satellite remote sensing data used to establish forest age in this study have long gaps in coverage (Helmer et al., 2008) that contribute to uncertainty in estimates of forest age, and thus on biomass accumulation rates, especially for the older forest classes. Recent studies have used dense time series of satellite data to track annual changes in forest cover (Schwartz, Aide, Graesser, Grau, & Uriarte, 2020; Silva Junior et al., 2020), but these studies primarily target younger second-growth forests, since Landsat or comparable data are not available on an annual basis before the mid-1980s. Forest age is also difficult to assess in the field. For example, remnant shade trees within second-growth forests regenerating after coffee or pasture complicate the estimation of forest age, and the presence (or absence) of woody vegetation influences initial AGB and forest succession. Finally, the cumulative impact of both stand-replacing and non-stand-replacing disturbances also introduces uncertainty in estimates of forest age, especially for older second-growth forests. Despite the rich archive of historic air photos, satellite data, and forest inventory information, age since last disturbance is particularly difficult to quantify in Puerto Rico, as the island regularly experiences hurricane and tropical-storm force winds, and the cumulative structural damages from wind exposure may alter the age–biomass relationship.

Across Puerto Rico, the role of previous land uses on AGB accumulation in second-growth forests remains visible, even after five decades of regrowth. Forests that recovered after coffee had higher biomass than forests that recovered after pastures, consistent with previous studies in Puerto Rico (Aide, Zimmerman, Herrera, Rosario, & Serrano, 1995; Marcano-Vega et al., 2002; Pascarella et al., 2000). Coffee plantations have different starting conditions compared to pastures. Soil additions such as lime and fertilizer may have accelerated forest growth. Greater initial woody cover may also accelerate forest recovery by providing shade (Parrotta, 1992) and perching sites for animals that disperse seeds (Wunderle, 1997). Both factors may help explain faster biomass accumulation and residual differences in older forests, especially in areas of former shade coffee with a mixture of coffee and broadleaf species at the time of agricultural abandonment. On the other hand, continued grazing or browsing may inhibit the establishment of trees in pastures, slowing forest recovery (Helmer et al., 2010). Previous studies in Puerto Rico using field plot data indicate that, after 40–60 years, basal area and diversity in second-growth forests are similar to undisturbed sites. The large sample of second-growth forests in this study captured lingering differences in aboveground biomass among land use categories on the same substrate after five decades of forest regrowth, which warrants further investigation into the selective pressure of past land use on forest structure and composition.

Our study also revealed heterogeneous patterns of biomass accumulation across different substrates. In particular, we found slower biomass accumulation on ultramafic substrate, where, unexpectedly, biomass was higher in intermediate-aged forests than older forests. Ultramafic rocks in Puerto Rico are associated with serpentine soils with low nutrient content, resulting in shorter forests (Medina, Cuevas, Figueroa, & Lugo, 1994; Porder & Ramachandran, 2013). The pattern of intermediate-aged forests having more biomass than the oldest forest has also been observed in forest inventory data (Helmer et al., 2008). One possible explanation is that the oldest forests on ultramafic substrate are on the least productive sites. In Puerto Rico, agricultural areas on ultramafic substrate and in cloud forests were often the first to be abandoned (Helmer et al., 2008). In addition, rates of biomass accumulation were very similar on the two most common substrates, limestone and volcaniclastic, despite pronounced differences in nutrient availability and water holding capacity. This similarity has also been observed in previous work with inventory data in Puerto Rico (Helmer et al., 2008; Rivera & Aide, 1998). One possible explanation is that historic deforestation in the karst region was concentrated in valleys. These valley bottoms are more protected from storms, and the rugged topography allows water and organic matter to accumulate in valley sites, creating more suitable conditions for plant growth than other topographic positions (Muscarella, Kolyaie, Morton, Zimmerman, & Uriarte, 2020; Rivera & Aide, 1998). Further, we also found the plateau in biomass accumulation appears after 33 years based on the full dataset was less visible when looking at each substrate individually. This result underscores the need to capture landscape heterogeneity to accurately predict the potential for reforestation to contribute to climate change mitigation, including variability in forest recovery on different substrates.

Biomass also increased with precipitation, topographic wetness, and slope. Together, these three variables capture conditions needed to understand site conditions associated with water deficits and waterlogged soils. Some of this pattern may relate to land use. For example, coffee plantations were commonly established in wetter regions of Puerto Rico, and steep slopes were typically abandoned before flatter areas. Overall, however, positive relationships between biomass and precipitation, topographic wetness (represented in our study by the topographic wetness index, TWI), and slope follows the pattern found in other tropical regions (Becknell, Kissing Kucek, & Powers, 2012; Lewis et al., 2013; Malhi et al., 2006; Saatchi, Houghton, Dos Santos Alvalá, Soares, & Yu, 2007). Higher rainfall or water availability, measured as TWI, alleviates growth constraints up to the point where soils are waterlogged (Muscarella et al., 2020). Waterlogged conditions are less common in sloped environments, hence the positive association between biomass and all three factors.

Overall, we found that biomass in second-growth forests of Puerto Rico was 34% lower than other Neotropical forests of similar ages. In addition to the combined influence of prior land use, substrate, and topography, as noted above, factors related to disturbances and methodology likely contribute to this difference. First, demographic factors such as time since disturbance contribute to the unique stature, composition, and biomass of forests in Puerto Rico (Brokaw & Grear, 1991; Brokaw & Walker, 1991). Puerto Rican forests regularly experience wind events, including hurricanes and tropical storms, and cumulative structural damages from these non-stand-replacing disturbances are one factor that likely limits height growth and biomass accumulation. Age-related mortality is another demographic factor that may explain the similarity in biomass among forests of intermediate ages. The degree to which synchronized waves of land abandonment (Helmer et al., 2008) precipitate synchronous mortality of pioneer tree species is unknown. Stratification of FIA plot data by age may allow for a more detailed investigation of changes in pioneer tree species abundance and associated declines in AGB.

At least three methodological factors may also account for some of the difference between biomass in this study and previous assessments, such as Poorter et al. (2016). First, lidar–biomass relationships between canopy height and biomass saturate in all forest types (Longo et al., 2016). However, the FIA plot data in this study exhibit a similar saturation in estimated aboveground biomass with age, suggesting that the difference is not strictly methodological. Second, frequent disturbances in Puerto Rico may result in a more rapid saturation of height–biomass relationships than regions with fewer storms; indeed, evidence for regional height–diameter relationships (Hunter, Keller, Victoria, & Morton, 2013) point to the need for further refinement of allometric relationships use to estimate biomass. Differences in allometric models may account for some of the difference reported here. For example, even within FIA, biomass estimates using the volume-based approach can be lower

than those based on local allometric equations (9% lower in our case; data not shown). The growing use of terrestrial lidar in forest inventory (Moskal & Zheng, 2011) may enable more accurate, 3-D estimates of wood volume, an approach that may identify spatial and temporal differences in individual tree damage, especially in older forests. Third, lidar data in this study covered 16,788 ha, nearly 120-fold greater area sampled than a regional syntheses, or 4000-fold greater sampling than the average chronosequence study (e.g., Poorter et al., 2016). This greater sampling covers a broader range of forest conditions across the landscape to better capture biomass distributions and disturbance dynamics (Fisher, Hurtt, Thomas, & Chambers, 2008), especially in human-dominated landscapes.

Long-term studies of second-growth forests regeneration are rare in the tropics. We traded space for time to generate a very large sample that covered more than 16,000 ha and nearly 100 years. The downsides to this trade are the well-known drawbacks of the chronosequence approach. We implicitly assume that the initial conditions for regeneration and controlling processes are the same for all time periods. This is clearly not true. In earlier time periods, when most of the island was deforested, dispersal and seed source availability may have presented greater barriers to regeneration than at later times. Similarly, abandonment depends upon utility, and all other things being equal, less economically productive areas (steep slopes and infertile soils) will be abandoned first. These sites deemed unsuitable for agriculture start their regeneration with a nutrient debt, limiting the pace of regeneration (Davidson et al., 2007). Natural and anthropogenic disturbances also contribute to the complex reality of second-growth forests in human-dominated landscapes. Older second-growth tropical forests in other regions face similar conditions, with growing human pressure from rising population, forest fragmentation, and increasing frequency of extreme events, including intense rainfall events that may contribute to branch loss or treefall events. These realities suggest that carbon accumulation in second-growth forests may not be as rapid or as permanent as suggested by simple models developed to promote the effectiveness of natural climate solutions (e.g., Griscom et al., 2017).

Statistical modeling studies are also subject to limitations. Even with 16,000 ha of lidar data coverage, we were underpowered to consider rare classes (when stratified by age, substrate, land use, and topography), in particular young second-growth forests. Sample sizes also limited the ability to consider complex interactions among variables. The FIA data in this study are the best available data for a range of forest ages and conditions in Puerto Rico. However, FIA plots are small, in comparison to other calibration plots for lidar–biomass estimation (e.g., Asner et al., 2012), and this increases the potential bias because high-biomass plots may be influenced by only one or two large trees (Longo et al., 2016; White et al., 2013). In addition, field data collection and allometric equations also include errors, and we did not explicitly consider the grid cell-level biomass uncertainty when we developed the model of biomass controls. Thus, this study also highlights the need for more foundational work on error propagation, including specific attention to aspects of allometric uncertainty that most strongly influence lidar-based biomass

models. Finally, the combination of different sources of remotely sensed data can improving the mapping of AGB and the understanding of successional stages in second-growth tropical forests (Hernández-Stefanoni et al., 2020; Velasco-Murguía, del Castillo, Rös, & Rivera-García, 2021).

Fine-scale heterogeneity in the biomass of second-growth forests of Puerto Rico underscores the need to consider a broad range of factors that influence biomass accumulation. Here, we identified important controls on biomass accumulation by age, based on differences in prior land use, substrate, and topographic position. Differences within and across categories were persistent, even after an estimated 50+ years of regrowth, highlighting the need to account for these specific drivers in ecosystem models. Our study highlights the value of airborne lidar for quantifying biomass variability in complex tropical landscapes with cumulative impacts from both natural and human disturbance processes. Evidence for slower biomass accumulation in second-growth forests of Puerto Rico has important consequences for the total carbon storage and expected climate mitigation benefits of large-scale reforestation efforts.

DATA AVAILABILITY STATEMENT
The data that support the findings of this study are openly available in the NGEE Tropics Data Collection: https://doi.org/10.15486/ngt/1873506 (Martinuzzi et al., 2022).

ORCID
Sebastián Martinuzzi https://orcid.org/0000-0003-3433-0561
Dexter H. Locke https://orcid.org/0000-0003-2704-9720
María Uriarte https://orcid.org/0000-0002-0484-0758

REFERENCES

Aide, T. M., Zimmerman, J. K., Herrera, L., Rosario, M., & Serrano, M. (1995). Forest recovery in abandoned tropical pastures in Puerto Rico. *Forest Ecology and Management*, 77, 77–86. https://linkinghub.elsevier.com/retrieve/pii/037811279503576V

Aide, T. M., Zimmerman, J. K., Pascarella, J. B., Rivera, L., & Marcano-Vega, H. (2000). Forest regeneration in a Chronosequence of tropical abandoned pastures: Implications for restoration ecology. *Restoration Ecology*, 8, 328–338. http://doi.wiley.com/10.1046/j.1526-100x.2000.80048.x

Aide, T. M., Zimmerman, J. K., Rosario, M., & Marcano, H. (1996). Forest recovery in abandoned cattle pastures along an elevational gradient in northeastern Puerto Rico. *Biotropica*, 28, 537. https://www.jstor.org/stable/2389095?origin=crossref

Andersen, H. E., Reutebuch, S. E., McGaughey, R. J., d'Oliveira, M. V. N., & Keller, M. (2014). Monitoring selective logging in western Amazonia with repeat lidar flights. *Remote Sensing of Environment*, 151, 157–165. https://doi.org/10.1016/j.rse.2013.08.049

Anselin, L. (2005). *Exploring spatial data with GeoDaTM: A workbook*. Center for Spatially Integrated Social Science.

Arriaga, L. (2000). Types and causes of tree mortality in a tropical montane cloud forest of Tamaulipas, Mexico. *Journal of Tropical Ecology*, 16, 623–636. https://www.cambridge.org/core/product/identifier/S0266467400001619/type/journal_article

Arroyo-Rodríguez, V., Melo, F. P. L., Martínez-Ramos, M., Bongers, F., Chazdon, R. L., Meave, J. A., Norden, N., Santos, B. A., Leal, I. R., & Tabarelli, M. (2017). Multiple successional pathways in human-modified tropical landscapes: New insights from forest succession, forest fragmentation and landscape ecology research. *Biological Reviews*, 92, 326–340. http://doi.wiley.com/10.1111/brv.12231

Asner, G. P., Mascaro, J., Muller-Landau, H. C., Vieilledent, G., Vaudry, R., Rasamoelina, M., Hall, J. S., & van Breugel, M. (2012). A universal airborne LiDAR approach for tropical forest carbon mapping. *Oecologia*, 168, 1147–1160. http://link.springer.com/10.1007/s00442-011-2165-z

Bawiec, W. J. (1999). *Geology, geochemistry, geophysics, mineral occurrences and mineral resource assessment for the Commonwealth of Puerto Rico: U.S. Geological Survey Open-File Report 98–038*.

Bechtold, W. A., and Patterson, P. L. Eds. (2005). *The enhanced forest inventory and analysis program - national sampling design and estimation procedures. Gen. Tech. Rep. SRS-80. U.S. Department of Agriculture, Forest Service, Southern Research Station, Asheville, NC.*

Becknell, J. M., Keller, M., Piotto, D., Longo, M., Nara dos-Santos, M., Scaranello, M. A., Bruno de Oliveira Cavalcante, R., & Porder, S. (2018). Landscape-scale lidar analysis of aboveground biomass distribution in secondary Brazilian Atlantic Forest. *Biotropica*, 50, 520–530. http://doi.wiley.com/10.1111/btp.12538

Becknell, J. M., Kissing Kucek, L., & Powers, J. S. (2012). Aboveground biomass in mature and secondary seasonally dry tropical forests: A literature review and global synthesis. *Forest Ecology and Management*, 276, 88–95. https://linkinghub.elsevier.com/retrieve/pii/S0378112712002009

Bivand, R., & Piras, G. (2015). Comparing implementations of estimation methods for spatial econometrics. *Journal of Statistical Software*, 63, 1–36. http://www.jstatsoft.org/v63/i18/

Bonner, M. T. L., Schmidt, S., & Shoo, L. P. (2013). A meta-analytical global comparison of aboveground biomass accumulation between tropical secondary forests and monoculture plantations. *Forest Ecology and Management*, 291, 73–86. https://linkinghub.elsevier.com/retrieve/pii/S0378112712007001

Brokaw, N. V. L., & Grear, J. S. (1991). Forest structure before and after hurricane Hugo at three elevations in the Luquillo Mountains, Puerto Rico. *Biotropica*, 23, 386. https://www.jstor.org/stable/2388256?origin=crossref

Brokaw, N. V. L., & Walker, L. R. (1991). Summary of the effects of Caribbean hurricanes on vegetation. *Biotropica*, 23, 442. https://www.jstor.org/stable/2388264?origin=crossref

Chazdon, R. L. (2014). *Second growth: The promise of tropical Forest regeneration in an age of deforestation*. University of Chicago Press. http://www.bibliovault.org/BV.landing.epl?ISBN=9780226118079

Chazdon, R. L., R. L Chazdon, E.N Broadbent, D. M A Rozendaal, F. Bongers, A. M. A. Zambrano, T. M. Aide, P. Balvanera, J. M Becknell, V. Boukili, P. H S Brancalion, D. Craven, Jarcilene S Almeida, ..., Lourens Poorter (2016). Carbon sequestration potential of second-growth forest regeneration in the Latin American tropics. *Science Advances* 2, e1501639. https://advances.sciencemag.org/lookup/doi/10.1126/sciadv.1501639.

Cook, B. D., Corp, L. A., Nelson, R. F., Middleton, E. M., Morton, D. C., McCorkel, J. T., Masek, J. G., Ranson, K. J., Ly, V., & Montesano, P. M. (2013). NASA goddard's LiDAR, hyperspectral and thermal (G-LiHT) airborne imager. *Remote Sensing*, 5, 4045–4066.

Crk, T., Uriarte, M., Corsi, F., & Flynn, D. (2009). Forest recovery in a tropical landscape: What is the relative importance of biophysical, socioeconomic, and landscape variables? *Landscape Ecology*, 24, 629–642. http://link.springer.com/10.1007/s10980-009-9338-8

Daly, C., Helmer, E. H., & Quiñones, M. (2003). Mapping the climate of Puerto Rico, Vieques and Culebra. *International Journal of Climatology*, 23, 1359–1381. http://doi.wiley.com/10.1002/joc.937

Davidson, E. A., de Carvalho, C. J. R., Figueira, A. M., Ishida, F. Y., Ometto, J. P. H. B., Nardoto, G. B., Sabá, R. T., Hayashi, S. N., Leal, E. C., Vieira, I. C. G., & Martinelli, L. A. (2007). Recuperation of nitrogen cycling in Amazonian forests following agricultural abandonment. *Nature*, 447, 995–998. http://www.nature.com/articles/nature05900

Drake, J. B., Dubayah, R. O., Clark, D. B., Knox, R. G., Blair, J. B., Hofton, M. A., Chazdon, R. L., Weishampel, J. F., & Prince, S. (2002). Estimation of tropical forest structural characteristics, using large-footprint lidar. *Remote Sensing of Environment*, 79, 305–319.

Ene, L. T., Gobakken, T., Andersen, H. E., Næsset, E., Cook, B. D., Morton, D. C., Babcock, C., & Nelson, R. (2018). Large-area hybrid estimation of aboveground biomass in interior Alaska using airborne laser scanning data. *Remote Sensing of Environment*, 204, 741–755.

FAO. (2010). *Global Forest Resources Assessment 2010*. FAO.

Fisher, J. I., Hurtt, G. C., Thomas, R. Q., & Chambers, J. Q. (2008). Clustered disturbances lead to bias in large-scale estimates based on forest sample plots. *Ecology Letters*, 11, 554–563. https://onlinelibrary.wiley.com/doi/10.1111/j.1461-0248.2008.01169.x

Flynn, D. F. B., Uriarte, M., Crk, T., Pascarella, J. B., Zimmerman, J. K., Aide, T. M., & Caraballo Ortiz, M. A. (2010). Hurricane disturbance alters secondary Forest recovery in Puerto Rico. *Biotropica*, 42, 149–157. https://onlinelibrary.wiley.com/doi/10.1111/j.1744-7429.2009.00581.x

Franco, P., Weaver, P., and Eggen-McIntosh, S. (1997). *Forest resources of Puerto Rico, 1990*.

Gobakken, T., Næsset, E., Nelson, R., Bollandsås, O. M., Gregoire, T. G., Ståhl, G., Holm, S., Ørka, H. O., & Astrup, R. (2012). Estimating biomass in Hedmark County, Norway using national forest inventory field plots and airborne laser scanning. *Remote Sensing of Environment*, 123, 443–456. https://linkinghub.elsevier.com/retrieve/pii/S0034425712001885

Griscom, B. W., Adams, J., Ellis, P. W., Houghton, R. A., Lomax, G., Miteva, D. A., Schlesinger, W. H., Shoch, D., Siikamäki, J. V., Smith, P., Woodbury, P., Zganjar, C., Blackman, A., Campari, J., ... Fargione, J. (2017). Natural climate solutions. *Proceedings of the National Academy of Sciences*, 114, 11645–11650. http://www.pnas.org/lookup/doi/10.1073/pnas.1710465114

Hansen, M. C., Potapov, P. V., Moore, R., Hancher, M., Turubanova, S. A., Tyukavina, A., Thau, D., Stehman, S. V., Goetz, S. J., Loveland, T. R., Kommareddy, A., Egorov, A., Chini, L., Justice, C. O., & Townshend, J. R. G. (2013). High-resolution global maps of 21st-century Forest

cover change. *Science (80-)*, *342*, 850–853. http://www.science-mag.org/cgi/doi/10.1126/science.1244693

Hansen, M. C., Wang, L., Song, X.-P., Tyukavina, A., Turubanova, S., Potapov, P. V., & Stehman, S. V. (2020). The fate of tropical forest fragments. *Science Advances*, *6*, eaax8574. https://advances.sci-encemag.org/lookup/doi/10.1126/sciadv.aax8574

Heath, L. S., Hansen, M., Smith, J. E., and Miles, P. D. (2009). Investigation into calculating tree biomass and carbon in the FIADB using a biomass expansion factor approach. In W. McWilliams, G. Moisen, and R. Czaplewski (Eds.), *Forest inventory and analysis (FIA) symposium 2008; October 21–23, 2008; Park City, UT. Proc. RMRS-P-56CD*. p. 26, U.S. Department of Agriculture, Forest Service, Rocky Mountain Research Station, Fort Collins, CO.

Helmer, E. H., Brandeis, T. J., Lugo, A. E., & Kennaway, T. (2008). Factors influencing spatial pattern in tropical forest clearance and stand age: Implications for carbon storage and species diversity. *Journal of Geophysical Research – Biogeosciences*, *113*, G02S04. http://doi.wiley.com/10.1029/2007JG000568

Helmer, E. H., Lefsky, M. A., & Roberts, D. (2009). Biomass accumulation rates of Amazonian secondary forest and biomass of old-growth forests from Landsat time series and the geoscience laser altimeter system. *Journal of Applied Remote Sensing*, *3*, 033505. http://remote-sensing.spiedigitallibrary.org/article.aspx?doi=10.1117/1.3082116

Helmer, E. H., Ruzycki, T. S., Wunderle, J. M., Vogesser, S., Ruefenacht, B., Kwit, C., Brandeis, T. J., & Ewert, D. N. (2010). Mapping tropical dry forest height, foliage height profiles and disturbance type and age with a time series of cloud-cleared Landsat and ALI image mosaics to characterize avian habitat. *Remote Sensing of Environment*, *114*, 2457–2473. https://linkinghub.elsevier.com/retrieve/pii/S003442571000177X

Hernández-Stefanoni, J. L., Castillo-Santiago, M. Á., Mas, J. F., Wheeler, C. E., Andres-Mauricio, J., Tun-Dzul, F., George-Chacón, S. P., Reyes-Palomeque, G., Castellanos-Basto, B., Vaca, R., & Dupuy, J. M. (2020). Improving aboveground biomass maps of tropical dry forests by integrating LiDAR, ALOS PALSAR, climate and field data. *Carbon Balance and Management*, *15*, 15. https://cbmjournal.biomedcentral.com/articles/10.1186/s13021-020-00151-6

Huang, W., Dolan, K., Swatantran, A., Johnson, K., Tang, H., O'Neil-Dunne, J., Dubayah, R., & Hurtt, G. (2019). High-resolution mapping of aboveground biomass for forest carbon monitoring system in the tri-state region of Maryland, Pennsylvania and Delaware, USA. *Environmental Research Letters*, *14*, 095002. https://iopscience.iop.org/article/10.1088/1748-9326/ab2917

Hudak, A. T., Strand, E. K., Vierling, L. A., Byrne, J. C., Eitel, J. U. H., Martinuzzi, S., & Falkowski, M. J. (2012). Quantifying aboveground forest carbon pools and fluxes from repeat LiDAR surveys. *Remote Sensing of Environment*, *123*, 25–40.

Hunter, M. O., Keller, M., Victoria, D., & Morton, D. C. (2013). Tree height and tropical forest biomass estimation. *Biogeosciences*, *10*, 8385–8399. https://bg.copernicus.org/articles/10/8385/2013/

Kennaway, T., & Helmer, E. H. (2007). The forest types and ages cleared for land development in Puerto Rico. *GIScience Remote Sens.*, *44*, 356–382. https://www.tandfonline.com/doi/full/10.2747/1548-1603.44.4.356

Kutner, M. H., Nachtsheim, C. J., Neter, J., & Li, W. (2005). *Applied linear statistical models* (5th ed.). McGraw-Hill.

Lasky, J. R., Uriarte, M., Boukili, V. K., Erickson, D. L., Kress, W. J., & Chazdon, R. L. (2014). The relationship between tree biodiversity and biomass dynamics changes with tropical forest succession M. Vila (Ed.). *Ecology Letters*, *17*, 1158–1167. http://doi.wiley.com/10.1111/ele.12322

Letcher, S. G., & Chazdon, R. L. (2009). Rapid recovery of biomass, species richness, and species composition in a Forest Chronosequence in northeastern Costa Rica. *Biotropica*, *41*, 608–617. https://onlinelibrary.wiley.com/doi/10.1111/j.1744-7429.2009.00517.x

Lewis, S. L., Sonké, B., Sunderland, T., Begne, S. K., Lopez-Gonzalez, G., van der Heijden, G. M. F., Phillips, O. L., Affum-Baffoe, K., Baker, T. R., Banin, L., Bastin, J.-F., Beeckman, H., Boeckx, P., Bogaert, J., De Cannière, C., Chezeaux, E., Clark, C. J., Collins, M., Djagbletey, G., … Zemagho, L. (2013). Above-ground biomass and structure of 260 African tropical forests. *Philosophical Transactions of the Royal Society B: Biological Sciences*, *368*, 20120295. https://royalsociety-publishing.org/doi/10.1098/rstb.2012.0295

Longo, M., Keller, M., dos-Santos, M. N., Leitold, V., Pinagé, E. R., Baccini, A., Saatchi, S., Nogueira, E. M., Batistella, M., & Morton, D. C. (2016). Aboveground biomass variability across intact and degraded forests in the Brazilian Amazon. *Global Biogeochemical Cycles*, *30*, 1639–1660.

Malhi, Y., Wood, D., Baker, T. R., Wright, J., Phillips, O. L., Cochrane, T., Meir, P., Chave, J., Almeida, S., Arroyo, L., Higuchi, N., Killeen, T. J., Laurance, S. G., Laurance, W. F., Lewis, S. L., Monteagudo, A., Neill, D. A., Vargas, P. N., Pitman, N. C. A., … Vinceti, B. (2006). The regional variation of aboveground live biomass in old-growth Amazonian forests. *Global Change Biology*, *12*, 1107–1138. https://onlinelibrary.wiley.com/doi/10.1111/j.1365-2486.2006.01120.x

Marcano-Vega, H., Aide, T. M., & Báez, D. (2002). Forest regeneration in abandoned coffee plantations and pastures in the cordillera central of Puerto Rico. *Plant Ecology*, *161*, 75–87.

Martinuzzi, S., Cook, B., Helmer, E., Keller, M., Locke, D., Marcano-Vega, H., Uriarte, M., & Morton, D. (2022). Patterns and controls on island-wide aboveground biomass accumulation in second-growth forests of Puerto Rico. 1.0. NGEE Tropics Data Collection (dataset). https://doi.org/10.15486/ngt/1873506

Mascaro, J., Asner, G. P., Dent, D. H., DeWalt, S. J., & Denslow, J. S. (2012). Scale-dependence of aboveground carbon accumulation in secondary forests of Panama: A test of the intermediate peak hypothesis. *Forest Ecology and Management*, *276*, 62–70. https://linkinghub.elsevier.com/retrieve/pii/S0378112712001995

Medina, E., Cuevas, E., Figueroa, J., & Lugo, A. E. (1994). Mineral content of leaves from trees growing on serpentine soils under contrasting rainfall regimes in Puerto Rico. *Plant and Soil*, *158*, 13–21. http://link.springer.com/10.1007/BF00007912

Metcalfe, P., Beven, K., & Freer, J. (2015). Dynamic TOPMODEL: A new implementation in R and its sensitivity to time and space steps. *Environmental Modelling and Software*, *72*, 155–172. https://linkinghub.elsevier.com/retrieve/pii/S1364815215001735

Miller, A. J. (1984). Selection of subsets of regression variables. *Journal of the Royal Statistical Society, Series A*, *147*, 389. https://www.jstor.org/stable/10.2307/2981576?origin=crossref

Moskal, L. M., & Zheng, G. (2011). Retrieving forest inventory variables with terrestrial laser scanning (TLS) in urban heterogeneous forest. *Remote Sensing*, *4*, 1–20. http://www.mdpi.com/2072-4292/4/1/1

Muscarella, R., Kolyaie, S., Morton, D. C., Zimmerman, J. K., & Uriarte, M. (2020). Effects of topography on tropical forest structure depend on climate context T. Jucker (Ed.). *Journal of Ecology*, *108*, 145–159. https://onlinelibrary.wiley.com/doi/10.1111/1365-2745.13261

Nelson, R., Margolis, H., Montesano, P., Sun, G., Cook, B., Corp, L., Andersen, H. E., de Jong, B., Pellat, F. P., Fickel, T., Kauffman, J., & Prisley, S. (2017). Lidar-based estimates of aboveground biomass in the continental US and Mexico using ground, airborne, and satellite observations. *Remote Sensing of Environment*, *188*, 127–140. https://doi.org/10.1016/j.rse.2016.10.038

NOAA. (2017). *C-CAP Land Cover, Puerto Rico, 2010.*

Norden, N., Angarita, H. A., Bongers, F., Martínez-Ramos, M., Granzow-de la Cerda, I., van Breugel, M., Lebrija-Trejos, E., Meave, J. A., Vandermeer, J., Williamson, G. B., Finegan, B., Mesquita, R., & Chazdon, R. L. (2015). Successional dynamics in neotropical forests are as uncertain as they are predictable. *Proceedings of the National Academy of Sciences*, *112*, 8013–8018. http://www.pnas.org/lookup/doi/10.1073/pnas.1500403112

Nunes, S., Oliveira, L., Siqueira, J., Morton, D. C., & Souza, C. M. (2020). Unmasking secondary vegetation dynamics in the Brazilian Amazon. *Environmental Research Letters*, 15, 034057. https://iopscience.iop.org/article/10.1088/1748-9326/ab76db

Orihuela-Belmonte, D. E., de Jong, B. H. J., Mendoza-Vega, J., Van der Wal, J., Paz-Pellat, F., Soto-Pinto, L., & Flamenco-Sandoval, A. (2013). Carbon stocks and accumulation rates in tropical secondary forests at the scale of community, landscape and forest type. *Agriculture, Ecosystems and Environment*, 171, 72–84. https://linkinghub.elsevier.com/retrieve/pii/S016788091300087X

Pan, Y., Birdsey, R. A., Fang, J., Houghton, R., Kauppi, P. E., Kurz, W. A., Phillips, O. L., Shvidenko, A., Lewis, S. L., Canadell, J. G., Ciais, P., Jackson, R. B., Pacala, S. W., McGuire, A. D., Piao, S., Rautiainen, A., Sitch, S., & Hayes, D. (2011). A large and persistent carbon sink in the World's forests. *Science (80-.)*, 333, 988–993. https://www.sciencemag.org/lookup/doi/10.1126/science.1201609

Parrotta, J. A. (1992). The role of plantation forests in rehabilitating degraded tropical ecosystems. *Agriculture, Ecosystems and Environment*, 41, 115–133. https://linkinghub.elsevier.com/retrieve/pii/016788099290105K

Pascarella, J. B., Aide, T. M., Serrano, M. I., & Zimmerman, J. K. (2000). Land-use history and Forest regeneration in the Cayey Mountains, Puerto Rico. *Ecosystems*, 3, 217–228. http://link.springer.com/10.1007/s100210000021

Poorter, L., Bongers, F., Aide, T. M., Almeyda Zambrano, A. M., Balvanera, P., Becknell, J. M., Boukili, V., Brancalion, P. H. S., Broadbent, E. N., Chazdon, R. L., Craven, D., de Almeida-Cortez, J. S., Cabral, G. A. L., de Jong, B. H. J., Denslow, J. S., Dent, D. H., DeWalt, S. J., Dupuy, J. M., ... Rozendaal, D. M. A. (2016). Biomass resilience of neotropical secondary forests. *Nature*, 530, 211–214. http://www.nature.com/articles/nature16512

Porder, S., & Ramachandran, S. (2013). The phosphorus concentration of common rocks—A potential driver of ecosystem P status. *Plant and Soil*, 367, 41–55. http://link.springer.com/10.1007/s11104-012-1490-2

Rivera, L. W., & Aide, T. M. (1998). Forest recovery in the karst region of Puerto Rico. *Forest Ecology and Management*, 108, 63–75. https://linkinghub.elsevier.com/retrieve/pii/S0378112797003496

Rozendaal, D. M. A., Bongers, F., Aide, T. M., Alvarez-Dávila, E., Ascarrunz, N., Balvanera, P., Becknell, J. M., Bentos, T. V., Brancalion, P. H. S., Cabral, G. A. L., Calvo-Rodriguez, S., Chave, J., César, R. G., Denslow, J. S., Dent, D. H., DeWalt, S. J., Dupuy, J. M., Durán, S. M., Dutrieux, L. P., ... Poorter, L. (2019). Biodiversity recovery of neotropical secondary forests. *Science Advances*, 5, eaau3114. https://advances.sciencemag.org/lookup/doi/10.1126/sciadv.aau3114

Saatchi, S. S., Houghton, R. A., Dos Santos Alvalá, R. C., Soares, J. V., & Yu, Y. (2007). Distribution of aboveground live biomass in the Amazon basin. *Global Change Biology*, 13, 816–837. https://onlinelibrary.wiley.com/doi/10.1111/j.1365-2486.2007.01323.x

Schwartz, N. B., Aide, T. M., Graesser, J., Grau, H. R., & Uriarte, M. (2020). Reversals of reforestation across Latin America limit climate mitigation potential of tropical forests. *Frontiers in Forests and Global Change*, 3, 85. https://www.frontiersin.org/article/10.3389/ffgc.2020.00085/full

Schwartz, N. B., Budsock, A. M., & Uriarte, M. (2019). Fragmentation, forest structure, and topography modulate impacts of drought in a tropical forest landscape. *Ecology*, 100, e02677. https://onlinelibrary.wiley.com/doi/10.1002/ecy.2677

Schwarz, G. (1978). Estimating the dimension of a model. *The Annals of Statistics*, 6, 461–464. http://projecteuclid.org/euclid.aos/1176344136

Sheridan, R. D., Popescu, S. C., Gatziolis, D., Morgan, C. L. S., & Ku, N. W. (2015). Modeling forest aboveground biomass and volume using airborne LiDAR metrics and forest inventory and analysis data in the Pacific northwest. *Remote Sensing*, 7, 229–255.

Silva Junior, C. H. L., Heinrich, V. H. A., Freire, A. T. G., Broggio, I. S., Rosan, T. M., Doblas, J., Anderson, L. O., Rousseau, G. X., Shimabukuro, Y. E., Silva, C. A., House, J. I., & Aragão, L. E. O. C. (2020). Benchmark maps of 33 years of secondary forest age for Brazil. *Science Data*, 7, 269. https://www.nature.com/articles/s41597-020-00600-4

Velasco-Murguía, A., del Castillo, R. F., Rös, M., & Rivera-García, R. (2021). Successional pathways of post-milpa fallows in Oaxaca, Mexico. *Forest Ecology and Management*, 500, 119644. https://linkinghub.elsevier.com/retrieve/pii/S0378112721007349

White, J. C., Wulder, M. A., Varhola, A., Vastaranta, M., Coops, N. C., Cook, B. D., Pitt, D., & Woods, M. (2013). A best practices guide for generating forest inventory attributes from airborne laser scanning data using an area-based approach. *The Forestry Chronicle*, 89, 722–723. http://pubs.cif-ifc.org/doi/10.5558/tfc2013-132

Woodall, C. W., Heath, L. S., Domke, G. M., and Nichols, M. C. (2011). *Methods and equations for estimating aboveground volume, biomass, and carbon for trees in the U.S. forest inventory, 2010. Gen. Tech. Rep. NRS-88. U.S. Department of Agriculture, Forest Service, Northern Research Station, Newtown Square, PA.* https://www.fs.usda.gov/treesearch/pubs/39555.

Wunderle, J. M. (1997). The role of animal seed dispersal in accelerating native forest regeneration on degraded tropical lands. *Forest Ecology and Management*, 99, 223–235. https://linkinghub.elsevier.com/retrieve/pii/S0378112797002089

Zarin, D. J., Davidson, E. A., Brondizio, E., Vieira, I. C. G., Sa, T., Feldpausch, T., Schuur, E. A. G., Mesquita, R., Moran, E., Delamonica, P., Ducey, M. J., Hurtt, G. C., Salimon, C., & Denich, M. (2005). Legacy of fire slows carbon accumulation in Amazonian Forest regrowth. *Frontiers in Ecology and the Environment*, 3, 365. http://doi.wiley.com/10.2307/3868585

SUPPORTING INFORMATION

Additional supporting information can be found online in the Supporting Information section at the end of this article.